**TECHNISCHE
UNIVERSITÄT
DRESDEN**

Alpha Decay Material Screening for Application in Ultra-Low-Background Experiments

Bachelor-Arbeit
zur Erlangung des Hochschulgrades
Bachelor of Science
im Bachelor-Studiengang Physik

vorgelegt von

Maximilian Cott
geboren am 01.06.2004 in Friedrichroda

Institut für Kern- und Teilchenphysik
Technische Universität Dresden

2025

Eingereicht am 04.08.2025

Abstract

For projects like the LEGEND experiment, in which very rare events are investigated, a detailed analysis of all possible background sources is crucial to obtain a valuable result. Amongst the potential sources of background in this experiment are the components of the experimental setup. It is important to radioassay these components to quantify the potential background they induce and to ensure high levels of radiopurity. The α-chamber at TU Dresden is a great asset to investigate the alpha-radiation emitted from the surface of such components.

Before the α-chamber can be used for the purpose of material screening, several preparation steps are necessary to make such a material screening possible. The goal of this work is to go these steps in the preparation. First a calibration is executed, which enables to match output values of the system to the energies of detected alpha-particles. After that simulations of the ionization of the used P5 gas with various α-energies are run, with the goal to find the top position of the ionization cloud and the center of charge. The purpose of this measure is to determine the energy-dependent parameters of the position cut and the drift velocity cut, which reduce the background of the alpha-chamber itself. The last step is the evaluation of the background spectrum of the chamber. Contaminants are identified and their activity quantified, with the two goals of being able to distinguish these events from sample events and to reduce the background in the long run.

Zusammenfassung

Für Projekte wie das LEGEND-Experiment, in denen seltene Ereignisse beobachtet werden sollen, ist es von enormer Bedeutung, eine detaillierte Analyse der Hintergrundereignisse durchzuführen. Zu den potenziellen Quellen für Hintergrundereignisse zählen unter anderem die Bauteile des Versuchsaufbaus selbst. Deswegen ist eine wichtige Aufgabe in solchen Projekten, die Vermessung solcher Bauteile. Die α-Kammer an der TU Dresden eignet sich hervorragend für die Untersuchung von α-Teilchen, die Teil der vielfältigen Störereignisse sind.

Bevor die α-Kammer für solche Untersuchungen genutzt werden kann müssen einige Maßnahmen der Vorbereitung erfolgen. Zunächst muss das Gerät kalibriert werden, um gemessene Werte den passenden Energien zuordnen zu können. Ein nächster Schritt ist das Definieren von automatischen Datenfiltern, die Ereignisse verursacht von den Proben von Ereignissen, die wiederum dem Hintergrund der α-Kammer zugehörig sind zu unterscheiden. Als letztes wird noch der Hintergrund der α-Kammer selbst ausgewertet, mit dem Ziel Ereignisse, die nicht zu den Proben gehören identifizieren und auf lange Sicht ihr Auftreten vermindern zu können.

Contents

1   Introduction

An expansion of the standard model of particle physics is, neutrinos being majorana particle, which means they are their own anti particles. Next to other effects this would allow the neutrinoless double beta decay. However, due to the small mass of neutrinos, neutrinoless double beta decay is a very rare process, which requires experiments with very low background levels. One of these experiments is the LEGEND experiment, which uses HPGe detectors enriched in ^{76}Ge for the search for neutrinoless double beta decay. The LEGEND experiment wants to reach a sensitivity for events with a half-life up to 10^{28} years [1]. The reduction of background radation is attempted in various ways. The first factor is the location of the setup under the Gran Sasso in Italy, reducing the background stemming from cosmic muons by a factor of 10^6 [2]. Another very important step is the use of highly radiopure materials in the setup itself. The several types of radiation α, β and γ are examined in different screening setups.

At the institute of nuclear and particle physics at the Technical University Dresden, an instrument of use is the twin Frisch-grid ionization chamber. With this instrument, which in this work will be referred to as α-chamber, it is possible to detect alpha particles and determine their energy. This work will go the steps in the preparation of the α-chamber for the screening of elements of the Legend experiment.

In chapter 2 first the underlying principles of the α-decay and then the most important information about the process of detection and data analysis are discussed. In chapter 3 the chamber is calibrated using 2 sources with a well known emission energy. Chapter 4 has the goal of adjusting the energy-dependent factors in the position cut and drift velocity cut to the now used P5 gas, which shall correctly distinguish the environmental background of the alpha chamber from events induced by the measured/screened sample. For this purpose, simulations of the development of charge clouds are executed. From these simulations the top position and the center of charge of these clouds is obtained. The ratio between these two properties is important to modify an equation used as a data filter. If the goal is to identify radiation coming from samples of the LEGEND setup it is necessary to distinguish these from the background in the chamber. Therefore the last task, discussed in chapter 5, is to identify contamination sources in the background spectrum.

2 Theory

2.1 α-Decay

α-Decay is the process of an atomic nucleus emitting 2 protons and 2 neutrons (a helium nucleus). Therefore the general nuclear reaction equation is:

$$^{A}_{Z}X_N \rightarrow ^{A-4}_{Z-2}Y_{N-2} + ^{4}_{2}He_2$$
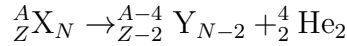
Just releasing nucleons often allows heavy nuclei to gain stability, that is why α-decaying isotopes can be found at the upper end of the nuclide chart.

2.1.1 The Decay Law

Nuclear decay is a statistical process that can be quantified by a simple differential equation. To gain intuition for this formula it can be useful to think of a specific isotope having a probability to decay in a short time dt of $p = \lambda dt$. In this case λ is a constant factor describing the statistical properties of the specific isotope. To ensure that p constitutes a probability (dimensionless, bigger than 0), λ also needs to greater than 0 and have the dimension $\frac{1}{time}$. To obtain an applicable law, we look at the change in the number of atoms $(-dN)$ as the expected value in the short time dt for N atoms. This leaves us with the well known ODE $-dN = N\lambda dt$. From this one can obtain the decline of the number of mother isotopes over time.

$$-dN = N\lambda dt \tag{1}$$

$$\frac{1}{N}dN = -\lambda dt \tag{2}$$

$$\int \frac{1}{N}dN = -\int \lambda dt \tag{3}$$

$$\ln|N| = -\lambda t + C \tag{4}$$

Because $N > 0$ the specification $|N|$ is just N

$$N(t) = e^{-\lambda t + C} \tag{5}$$

e^C equals N at $t = 0$. Therefore we define $N_0 := e^C$ as the initial number of atoms of the mother type.

$$N(t) = N_0 e^{-\lambda t} \tag{6}$$

To describe the behavior of a certain isotope, instead of the pragmatic use of λ, literature often refers to a more intuitive value: The half life $t_{1/2}$. This is the time, after which only half of the original atoms are left in the initial state. It can be expressed using λ as well:

$$N(t_{1/2}) = \frac{N_0}{2} \tag{7}$$

$$N_0 e^{-\lambda t_{1/2}} = \frac{N_0}{2} \tag{8}$$

$$e^{-\lambda t_{1/2}} = \frac{1}{2} \tag{9}$$

$$t_{1/2} = \frac{\ln 2}{\lambda} \tag{10}$$

[3]

2.1.2   QM-Process

The Q-value represents the total energy release. Because of energy conservation, it can also be expressed as the difference in the binding energies of mother nucleus and daughter nuclei. The binding energy of a nucleus can be described by:

$$E_b = a_v A - a_s A^{2/3} - a_c \frac{Z^2}{A^{1/3}} - a_A \frac{(A - 2Z)^2}{A} + \delta(N, Z) \tag{11}$$

or the mass defect:

$$Q = \Delta m\, c^2 \tag{12}$$

It provides a simple condition for the possibility of a decay. In order for the reaction to be possible, the Q-value must be positive.

When an α-particle is emitted, it has to overcome the Coulomb potential:

$$V_c = 2(Z - 2)\frac{e^2}{r} \tag{13}$$

which is higher than the energy E_α at the initial position of the α-particle.

The amplitude of the wavefunction decays exponentially in a section of $V > E$, therefore:

$$P \sim e^{-2\gamma} \quad \text{with} \quad \gamma = \int_{R_0}^{R_1} \sqrt{2m_\alpha(V(r) - E_\alpha)}\, dr \tag{14}$$

With R_0 the initial radial coordinate and R_1 the radius at which the potential gets lower than the energy.

Substitute in:

$$u = \frac{E_\alpha}{V(R)} \tag{15}$$

$$\gamma = 2(Z-2)\,\alpha\,\sqrt{\frac{2m_\alpha}{E_\alpha}}\int_{u_{\min}}^{1}\sqrt{\frac{1}{u}-1}\,du \tag{16}$$

$$\text{with}\quad u_{min} = \frac{E_\alpha}{V_{max}} = \frac{QR_0}{2(Z-2)\alpha} \tag{17}$$

This is the relation between amplitude of the wave function and Q-value. [3]

2.1.3   Kinematics

The Q-Value also allows a simple description of the kinetic energy of an emitted α-particle. For a mother nucleus X at rest, one receives for the energy conservation:

$$m_X c^2 = m_Y c^2 + T_Y + m_\alpha c^2 + T_\alpha \tag{18}$$

$$(m_X - m_Y - m_\alpha)c^2 = T_Y + T_\alpha \tag{19}$$

Using the Q-value gives:

$$Q = \left[m_X - (m_Y + m_\alpha)\right]c^2 \tag{20}$$

$$\Rightarrow Q = T_Y + T_\alpha \tag{21}$$

This allows to express the kinetic energy of an emitted α-particle using only the Q-value and the masses of the daughter Y and the α-particle. Using momentum conservation $p_Y = p_\alpha$ and that α-particles (and the daughter nuclei) can be described as non-relativistic, i.e. $T = \frac{p^2}{2m}$, leads to:

$$\sqrt{2m_Y T_Y} = \sqrt{2m_\alpha T_\alpha} \tag{22}$$

$$T_\alpha = \frac{m_Y}{m_\alpha} T_Y \tag{23}$$

with (21):

$$T_\alpha = \frac{m_Y}{m_\alpha}(Q - T_\alpha) \tag{24}$$

$$T_\alpha = \frac{Q}{1 + \frac{m_\alpha}{m_Y}} \tag{25}$$

[3]

2.1.4 Decay Chains

If a radioactive atom decays it is not uncommon for the resulting isotope - the daughter isotope - to also be unstable. In this way, cascades of different decay processes can be observed in measurement, even if only one radioactive isotope is initially present. This is an important process to consider when the goal is to analyze or to remove contamination in an experiment.

There is one particular chain of great interest for this work. The ^{238}U-chain, which components can be seen in figure one, among other isotopes, contains ^{222}Rn. This is a noble gas and can be released into the atmosphere during the decay process, which suggests, that ^{222}Rn and its daughters will contaminate the Chamber. The ^{222}Rn-chain, how the part of the ^{238}U-chain starting from ^{222}Rn will be referred to, was also detected in previous measurements [4]. The ^{222}Rn decay chain is shown in figure 2.1.
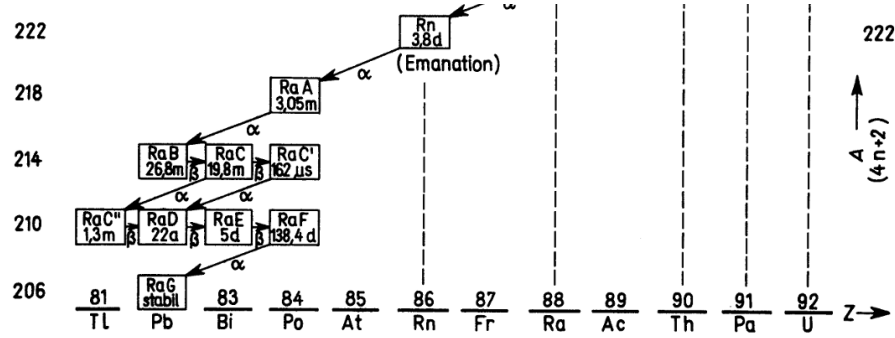

Figure 2.1: In this image the ^{222}Rn decay chain is shown [5].

Without a mother nuclide creating additional atoms the ODE describing the decay looks the same as in chapter 2.1.1.

$$\frac{dN_1}{dt} = -\lambda_1 N_1 \quad \Rightarrow \quad N_1(t) = N_{10}e^{-\lambda_1 t}, \quad N_{10} = N_1(0) \tag{26}$$

For any daughter nuclide we have to consider a loss of isotopes due to decay and a gain from decaying atoms of the mother nuclide:

$$\frac{dN_2}{dt} = -\lambda_2 N_2 + \lambda_1 N_1 = \lambda_1 N_{10}e^{-\lambda_1 t} - \lambda_2 N_2 \tag{27}$$

$$\frac{dN_2}{dt}e^{\lambda_2 t} + \lambda_2 N_2(t)e^{\lambda_2 t} = \lambda_1 N_{10}e^{-(\lambda_1 - \lambda_2)t} \tag{28}$$

$$\frac{d}{dt}\left(N_2(t)e^{\lambda_2 t}\right) = \lambda_1 N_{10}e^{-(\lambda_1 - \lambda_2)t} \tag{29}$$

$$N_2(t)e^{\lambda_2 t} = \frac{-\lambda_1}{\lambda_1 - \lambda_2}N_{10}e^{-(\lambda_1 - \lambda_2)t} + C \tag{30}$$

$$N_2(t) = \frac{-\lambda_1}{\lambda_1 - \lambda_2} N_{10} e^{-\lambda_1 t} + C e^{-\lambda_2 t} \tag{31}$$

C is worked out using the initial condition.

$$N_2(0) = N_{20} \tag{32}$$

$$C = N_{20} + \frac{\lambda_1}{\lambda_1 - \lambda_2} N_{10} \tag{33}$$

replace C:

$$N_2(t) = N_{20} e^{-\lambda_2 t} + \frac{\lambda_1}{\lambda_1 - \lambda_2} N_{10} (e^{-\lambda_2 t} - e^{-\lambda_1 t}) \tag{34}$$

If only one isotope of a chain is assumed to be the original contaminant, it would correspond to an initial condition of $N_{20} = 0$.

It would be useful to check rather the background shows the resulting behavior as ^{222}Rn appearing as a noble gas in the air is suspected to contaminate the chamber at every probe change. The resulting equation for a system with only atoms of the mother isotope is:

$$N_2(t) = \frac{\lambda_1}{\lambda_1 - \lambda_2} N_{10} \left(e^{-\lambda_2 t} - e^{-\lambda_1 t} \right) \tag{35}$$

[3]

Peak	E_α/MeV	$T_{1/2}$
^{222}Rn	5.590	3.82 d
^{218}Po	6.001	3.10 min
^{214}Pb	β-decay	27.06 min
^{214}Bi	β-decay	19.71 min
^{214}Po	7.689	163.3 μs
^{210}Pb	β-decay	22.20 y
^{210}Bi	β-decay	5.012 d
^{210}Po	5.304	138.4 d

Table 2.1: This table displays the half-lives of all isotopes in the ^{238}U chain, that are ^{222}Rn or its daughters. For the α-emitters the emission energy can also be seen.

[**IAEA**]

2.2   Important Principles for the Experimental Setup

An α-particle leaves its nucleus with a certain kinetic energy T_α (section 2.1.3). Before this energy of the α-particle can be detected, several steps have to be taken into account. The interaction of the α-particle with its surrounding matter as well as the signal creation and signal processing will be discussed in the following sections.

2.2.1 Deceleration of α-Particles in Matter

Before the energy of α-particles can be detected, several steps have to be taken into account. The interaction of the α- particle with its surrounding matter as well as the signal creation and signal processing will be discussed in the following sections. Therefore the first physical issue to be discussed should be, how and in what quantities high energetic particles loose energy, interacting with matter, especially gas [3].
Ions can deposit their energy via interaction in gas in two ways. The first is interaction with the electron shells of the gas atoms. The other possibility is collisions with the positively charged nuclei. The energy deposition into the nuclei is relatively small and often leads to emission of an electron later on, hence we can focus on shell interactions. To describe the behavior of a heavy particle like an α-particle, it is useful to look at the energy loss over disposition. The energy loss of an α-particle varies with the energy of the α-particle, which can be expressed with the Bethe-Bloch-equation [6]:

$$ -\left(\frac{dE}{dx}\right) = 4\pi N_a r_e^2 m_e c^2 \rho \frac{Zz^2}{AM_u\beta^2} \left[\frac{1}{2}\ln\left(\frac{2m_ec^2\beta^2\gamma^2T_{max}}{I}\right) - \beta^2 - \frac{\delta(\beta)}{2}\right] \quad (36) $$

The used quantities are:

- N_a: Avogadro's Constant
- r_e: classical radius of the electron
- Z: atomic number of gas atoms
- A: mass number of gas atoms
- M_u: molar mass constant
- m_e: electron mass

The most important characteristic is, that the energy loss reaches a peak at a low total energy (relatively low in comparison to the energies of the α-particles emitted in our experiments). The reason for this is the order of magnitude of the velocity at which the electrons travel in the shell. The general structure of these energy loss diagrams also has an interesting perk. If we look at a certain particle traveling in a certain medium, the only variable, that the energy loss over x depends on, is its own energy. Therefore diagrams depicting the energy loss of identical particles with different energies are exactly the same if viewed from the point, where the high energy particle reaches the initial energy of the one with lower energy. A good way to illustrate this to substitute the current energy of the particle with the range it is able to travel and to plot the energy deposition over that range.

2.2.2 Gaseous Detectors

After a particle is fully stopped, there is a charged cloud of free electrons in the chamber, which is accelerated towards the anode, by a voltage. The information, that can be extracted in the way, described at the beginning of the chapter, depends on the voltage used in the process.

If a voltage in the order of magnitude between $100\,\mathrm{V}$ and $1000\,\mathrm{V}$ is applied, the electrons do not gain enough energy to cause secondary ionization. Therefore the charge is not amplified. Detectors with this characteristic are called "Ionization Chambers" [6].

If the voltage is increased, the accelerated electrons will eventually gain the critical energy to cause secondary ionizations. The result is that more electrons reach the anode, than the number of electrons that was set free by the original particle. The factor between first order electrons and the total number of electrons increases exponentially at first. But this region of exponential increase can be divided in two, taking another effect into account.

The part of the problem that was illustrated, will probably create the intuition, that every electron causes the same amount of ionizations. Therefore the total number of electrons reaching the anode must be proportional to the number of electrons set free by the event particle itself. Up to a final number of 10^5 electrons, this is a useful approach. Because the initial number and final number of electrons are proportional to each other, the region of voltage is called the "Proportional regime".

If the voltage is increased further, another effect grows in relevance. The meaning of ionization is charge separation. A negatively charged electron is separated from an atom, which is now a positively charged ion. Both parts are accelerated in opposite directions. This causes the electric field to weaken. For Voltages around $3000\,\mathrm{V}$ the first electrons weaken the field so much, that the following electrons cause significantly fewer secondary ionizations. The number of initial and final electrons are no longer proportional. This region is therefore called the "Non-proportional regime".

For even higher voltages the number secondary ionizations grows so large, that the leftover ions cause the formation of secondary structures to stop. For some gases, a stable interval called the "Geiger regime" is reached.

In figure 2.2 you can see how the number of electrons reaching the anode varies for different voltages. On the y-axis the final number of electrons is shown. The initial number is 100 electrons for every voltage.

2.2.3 The α-Chamber

The α-chamber is a cylinder with a diameter of $d = 300\,\mathrm{mm}$. The bottom plate is removable for the purpose of changing probes. The anode is a circular plate
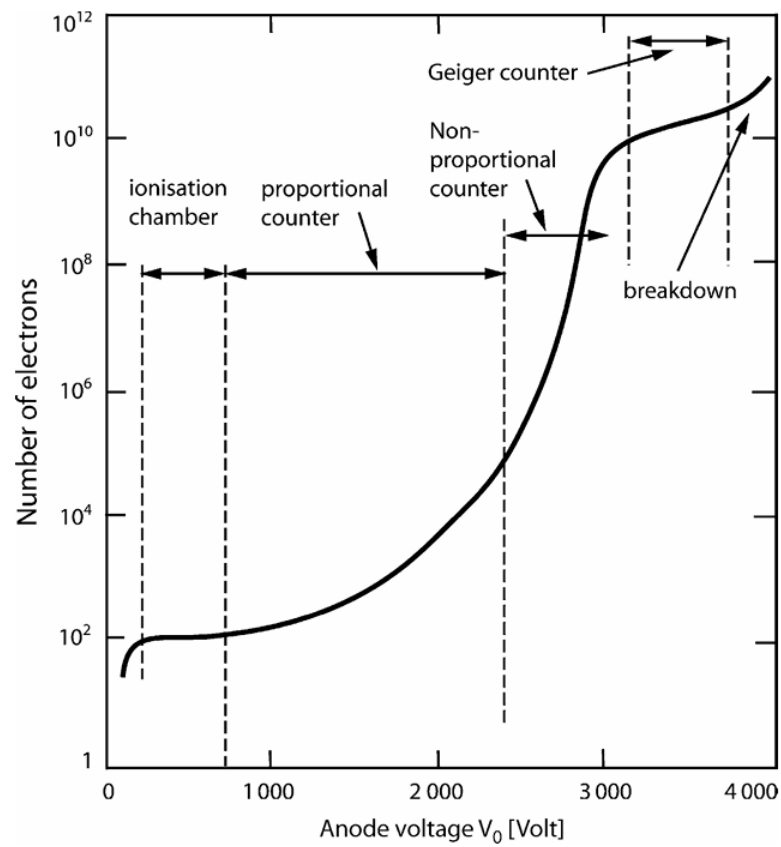
Figure 2.2: This diagram shows the different behavior of gas tubes for voltages between $0 - 4000\text{V}$. The graph displays the final number of electrons reaching the anode, for a number of 100 initial electrons set free by an event[7].
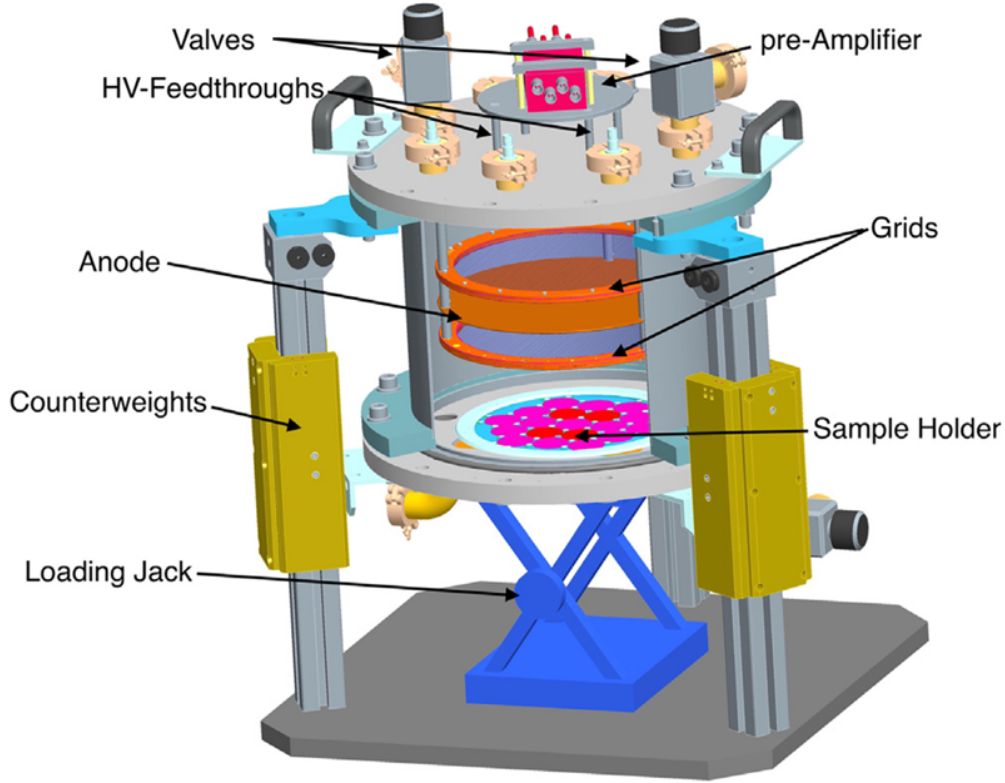
Figure 2.3: This image shows the α-chamber with its components[4].

positioned at half of the chambers hight. The bottom plate and the walls of the chamber are grounded and constitute the cathode. On each side of the anode above and below there is a grid. In the following sections these grids will be referred to as "upper grid" and "lower grid". The distance between anode and the grids is $h = 35\,\mathrm{mm}$. The lower grid sits $D = 100\,\mathrm{mm}$ above the cathode [4]. The inside is filled with P5-gas, which consists of 95% argon and 5% methane. The reason for the change from 10% methane, which was used in previous operations, is the reduced flammability of the gas. The walls and the base of the chamber are made out of aluminum, between base and sample a silicon waver is placed, as the used silicon is a radiopure material. A schematic drawing of the chamber can be seen in figure 2.3. The bottom plate is positioned on a loading jack and fixated with screws. On the metal rods fixating the chamber there are also counterweights ensuring, that the bottom plate can be moved upwards by hand. On top of the chamber there are valves connecting the inside to a vacuum pump and a gas tank containing P5. Also on top is the preamplifier and the connection to all other electronic devices. A schematic image of the whole system is shown in figure 2.4.
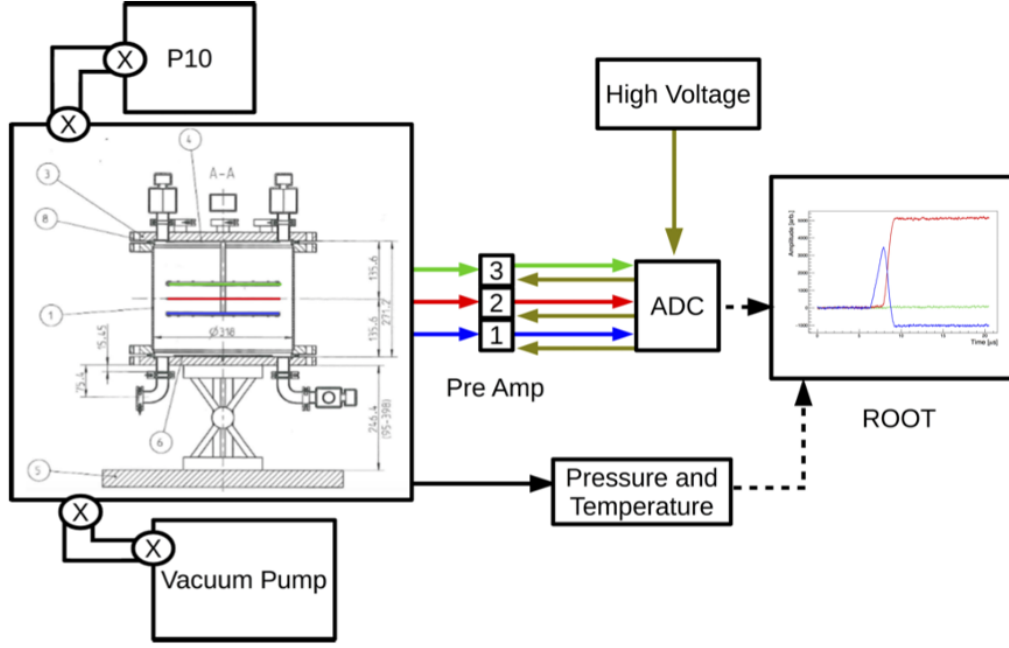
Figure 2.4: Here the complete setup, containing α-chamber, gas tank, vacuum pump and the first step of signal processing with the preamplifier and the connection to the server is shown[8].

2.2.4 Pulse Shapes

The detection principle is, that the separated electrons and ions induce a current on the anode, that can be measured. The system can the electric current at every point in time. The question left to answer is, how the electric current depends on the quantity and movement of the electrons and ions. A method to simulate the induced current on a conductor is suggested by *Shockley* [9] and *Ramo* [10]. It states that the charge induced at an electrode A is given by

$$Q_A = -q\phi_A(\vec{x}) \tag{37}$$

with a moving point charge q and the weighting potential $\phi_A(\vec{x})$. The weighting potential is the potential inside the chamber with the boundaries:
$\phi_A(\vec{x}) = 1$ at the anode A and $\phi_A(\vec{x}) = 0$ at all other electrodes.
For simplification a few assumptions are made: The induced current due to magnetic effects is assumed to be negligible and the electric field is assumed to propagate instantaneously [11].
The resulting pulse shapes for the charge clouds, created in the α-chamber, were simulated by Heinrich Wilsenach [8]. The conditions were identical except for the gas composition. In the simulation, P10 was used instead of P5, which is the gas mixture used in the experiments referenced in this work.

The pulse shapes were simulated for a chamber consisting of only a cathode and an anode (figure 2.5) and a recreation of the real experiment also containing a Frisch grid between anode and cathode (figure 2.6).
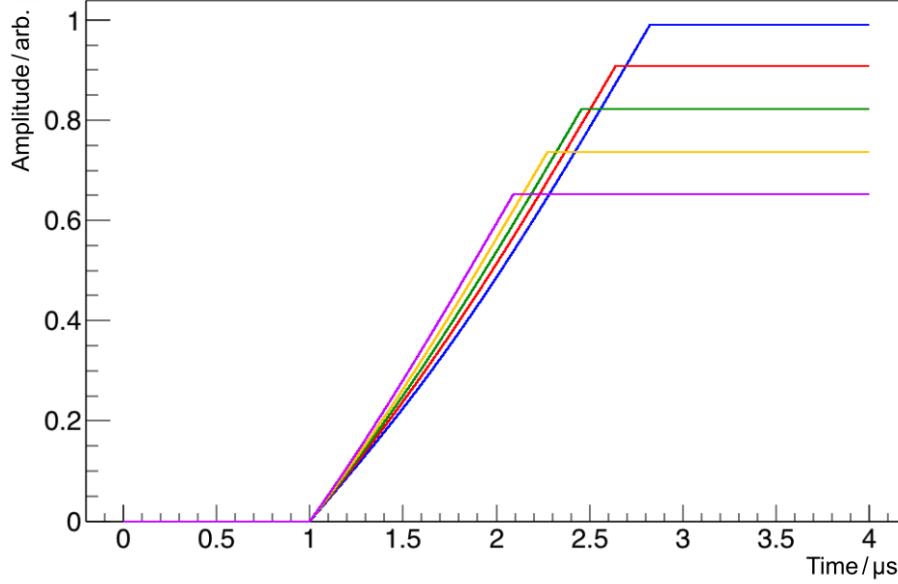

Figure 2.5: This image shows the resulting pulse shapes for a simulation of a simple chamber without grids[8].
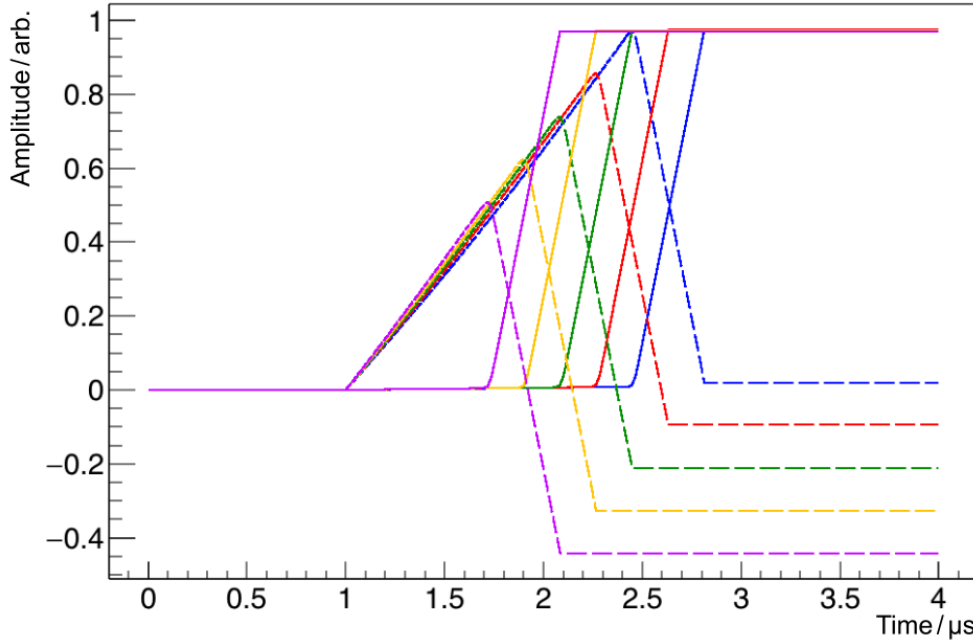

Figure 2.6: This image shows the resulting pulse shapes for a simulation of a chamber with Frisch grids[8].

2.2.5 Used Data Cuts

To obtain a scientifically useful spectrum from a measurement, a number of cut conditions is applied to the measured events. These cuts can be separated into two categories: Quality cuts discriminate alpha-events in the bottom part of the chamber from α-events in the upper part of the chamber, muonic events and non-physical events like noise. Physical cuts analyse the properties of an α-event to discriminate alpha-induced background from the signal events of the respective sample. Starting with the quality cuts, the following parts discuss the cut conditions applied to the measured events.

The first cut is that while lower grid (LG) and anode (A) need to be triggered, a signal on the upper grid (UG) leads to an exclusion of the event. The charges, set free by an α-particle only move between the bottom of the chamber and the anode. Therefore above the anode, where the upper grid is positioned, no signal should be detected. This cut primarily filters events created by the pulser, cosmic radiation and decays in the upper half of the chamber due to contamination. The conditions are:

$$t_{trig,A} > 0 \tag{38}$$

$$t_{trig,LG} > 0 \tag{39}$$

$$t_{trig,UG} = 0 \tag{40}$$

The second one focuses on the trigger times of the lower grid and the anode. The charge cloud is created in the interaction region, in other words: below the lower grid. Thus the cloud first passes the lower grid before traveling on to the anode and the lower grid pulse has its trigger time point before the corresponding pulse on the anode. This fact is exactly the content of the second condition.

$$t_{trig,A} - t_{trig,LG} > 0 \tag{41}$$

It filters out the events, where the anode was triggered first, which can be noise events or events triggered between lower grid and anode.

While these cuts seem rather simple, they are of great importance. They guarantee, that only α-events in the lower region of the chamber are accepted.

The next parameter to be discussed is the z-projection of the charge cloud's mean position. This parameter is denoted by $\frac{\bar{X}}{D}\cos\theta$. $\bar{X}$ is the distance between the position of the decay and the center of the charge cloud, θ is the angle of emission relative to the ground, resulting in the factor $\cos\theta = 1$ for a perfectly vertical track and D is the distance between chamber bottom and lower grid. The events of

interest are from the bottom of the chamber, thus $\bar{X}\cos\theta$ describes the z-position of the charge cloud. Because of the normalization using D, this is a dimensionless property. The projected position can be determined by the ratio between the final induced charges on the lower grid and the anode.

$$\frac{\bar{X}}{D}\cos\theta = -\frac{Q_{LG}}{Q_A} \tag{42}$$

Here Q_{LG} is the final induced charge on the lower grid and Q_A the one on the anode. The starting position of an α-particle is very important information when it comes to the development of cuts, because the particles from our source originate from the bottom of the α-chamber. When an alpha-particle is emitted from the bottom of the chamber, it can have a maximum z-projection $\frac{\bar{X}}{D}$. Events with a calculated z-projection larger than $\frac{\bar{X}}{D}$ cannot have their origin at the bottom of the detector and therefore can be excluded as background events. Such events are alphas emitted in the detectors gas volume, by ^{220}Rn and ^{222}Rn. In figure 2.7 the corresponding z-projection for a point charge, created by an α-particle, originated from the source is depicted.
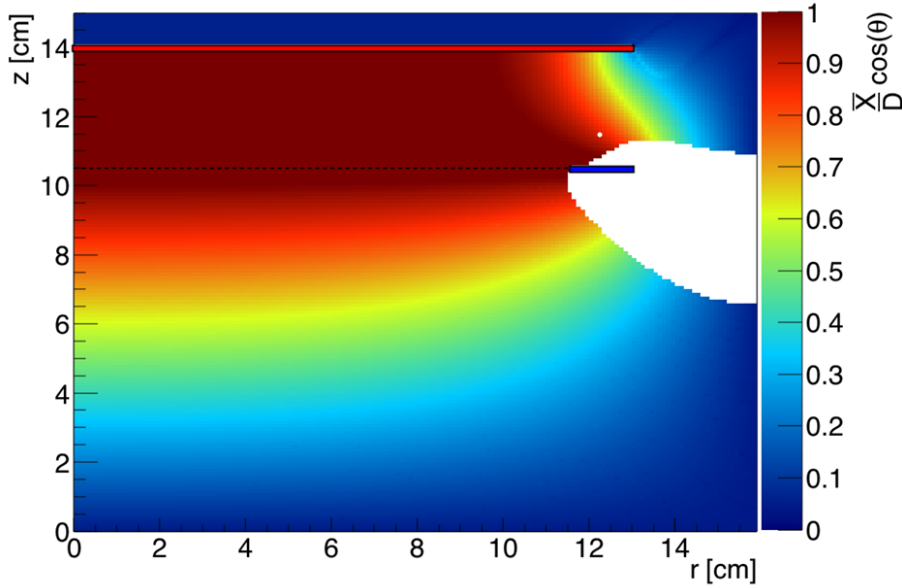

Figure 2.7: This image shows the z-projection value of a point charge in dependence of its point of origin[8].

It shows that while some event types can be filtered effectively, the model has flaws. Events with altered origins, especially the chamber wall can imitate source events. For that reason another filter, using the drift velocity as a cutting parameter, is implemented. The drift velocity of the electrons in a gas is determined by the gas properties and the electric field inside the chamber. In the central part of the chamber, where the samples are positioned, the electric field is almost constant

and only has small spatial variations. Assuming the drift velocity reaches saturation quickly, it can be described as constant as well. However the field is not homogeneous near the walls of the chamber, leading to a deviation from the calculated drift velocity. The electric field inside the chamber was simulated by Heinrich Wilsenach [8] and can be seen in figure 1.3.
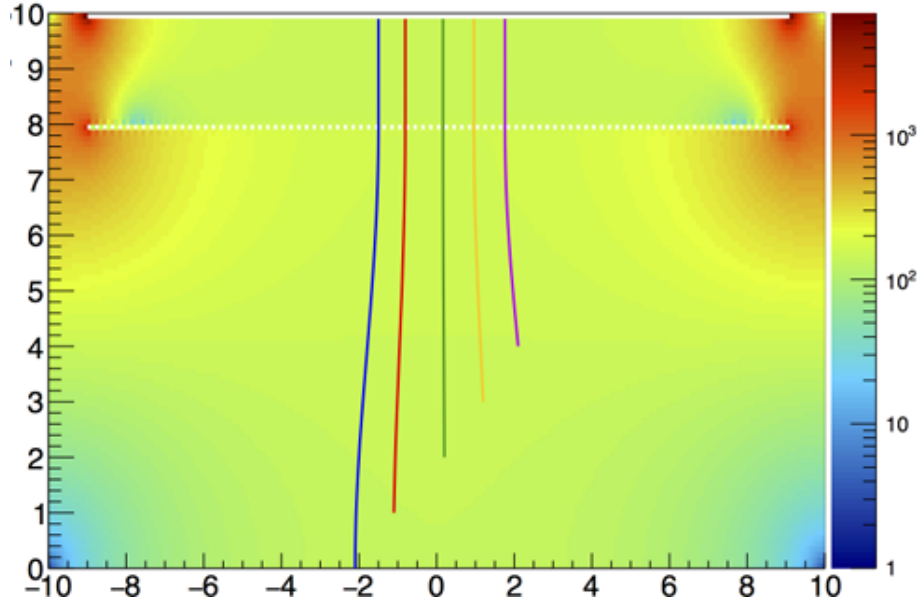

Figure 2.8: This image shows the result of a simulation of the electric field inside the chamber[8].

To determine the drift velocity, the position data of an event is combined with the trigger times of grid and anode. Their difference $(T_A - T_{LG})$ corresponds to the drift time the electrons need to reach the lower grid. The assigned values for trigger time of lower grid and anode (T_{LG}, T_A) are defined as the time the respective pulse reaches 20% of its own maximum. The mean velocity of an electron thus can be approximated with:

$$v_e = \frac{D - \bar{X} \cos \theta}{T_A - T_{LG}} \tag{43}$$

$$v_e = \frac{D \left(1 - \frac{\bar{X}}{D} \cos \theta\right)}{T_A - T_{LG}} \tag{44}$$

If a charge cloud is created instead of a point charge, the triggering times are sensitive to the maximum value of z-positions of the cloud. Therefore the z-projection in the equation (as $\frac{\bar{X}}{D} \cos \theta$ projects the mean position of the cloud) must be corrected: $\bar{X} \rightarrow X_{max}$. This correction factor a is energy dependent. This energy dependence

15

can be an intuitive result, if the general form of $(-\frac{dE}{dx})$ is taken into consideration. As the energy loss is exactly the same at the end of the stopping process and only the tail grows longer for higher energies, the mean value moves away from stopping point and Bragg peak [8].

3 Development of the Calibration

The first step to prepare the alpha chamber for a background measurement is the energy calibration. The idea for the calibration of the α-chamber is to measure the pulseheigts of at least two well known α-emitters. The calibration curve is then constructed using a fit ($f(ch) = a_1 ch + a_0$). The following will illustrate the process of evaluating the histograms containing the pulseheight distribution, extracting the peak values and the creation of the calibration curve.

3.1 Measurement

The data, used in all processes illustrated in this section, was obtained in previous measurements. The sources used were ^{241}Am and ^{148}Gd.

3.2 Fitting of the Pulseheight Distribution

The energy distribution of the emitted alphas and therefore distribution of the detected pulseheights can be described by the following function [12]:

$$f(E) = A \sum_{i=1}^{3} \frac{n_i}{2\tau_i} \exp\left(\frac{E-\mu}{\tau_i} + \frac{\sigma^2}{2\tau_i^2}\right) \text{erfc}\left(\frac{1}{\sqrt{2}}\left(\frac{E-\mu}{\sigma} + \frac{\sigma}{\tau_i}\right)\right) \tag{45}$$

- μ: peak position
- A: amplitude/ peak content
- σ: peak width
- τ_i: decay parameter of the low energy tail
- n_i: weighting parameters for the 3 components of the peak

This fit was implemented as a function and tested for altering initial values. The only fixated initial value was the one for the peak position. It was defined as the position of the bin with the highest counting rate. The test showed that the fit is unstable, meaning the functionality of the fitting algorithm heavily depends on the initial conditions. Especially the variation of the guess for the amplitude (A) showed great effect. Because of this dependence, the first step was to create a general algorithm that produces working initial values, in particular for A. The system used here includes two steps. First A is estimated using the integral over the bins of the histogram. After that a simpler form of the aforementioned function is applied. More precisely one of the linearly combined terms is used:

$$f(E) = \frac{A}{2\tau} \exp\left(\frac{E-\mu}{\tau} + \frac{\sigma^2}{2\tau^2}\right) \text{erfc}\left(\frac{1}{\sqrt{2}}\left(\frac{E-\mu}{\sigma} + \frac{\sigma}{\tau}\right)\right) \tag{46}$$

17

The 4 parameters in the simplified version are then used as the initial values:

$A = A_{simplified}$, $\mu = \mu_{simplified}$, $\sigma = \sigma_{simplified}$, $\tau_1 = \tau_{simplified}$

The other values for the τ_i were estimated with a value in the same order of magnitude. The scaling factors n_i were estimated as their variation does not impact the result for the further used parameters in a critical way.

After this procedure was implemented, the script was modified, so that multiple fits could be performed and the corresponding peak positions would be extracted. The resulting fits for the histograms are shown in figures 3.1, 3.2, 3.3 and 3.4
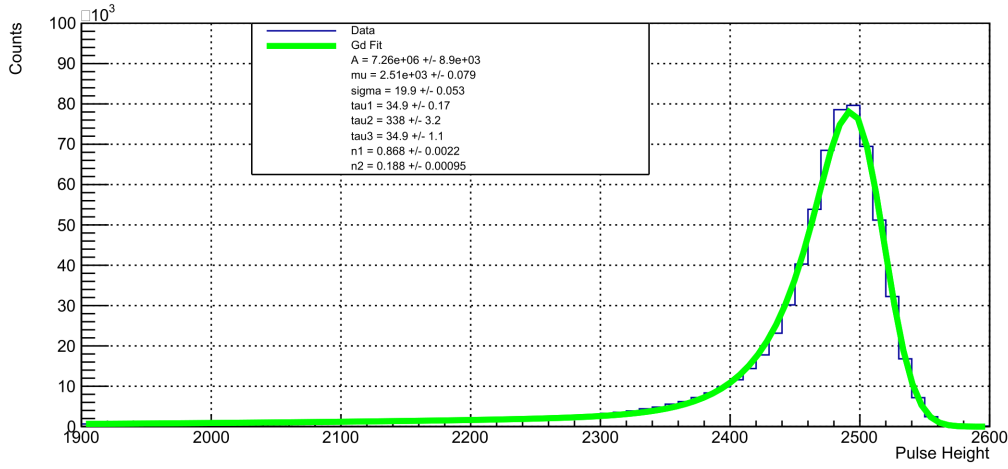

Figure 3.1: Histogram of the ^{148}Gd peak, with the α-fit produced as described above.
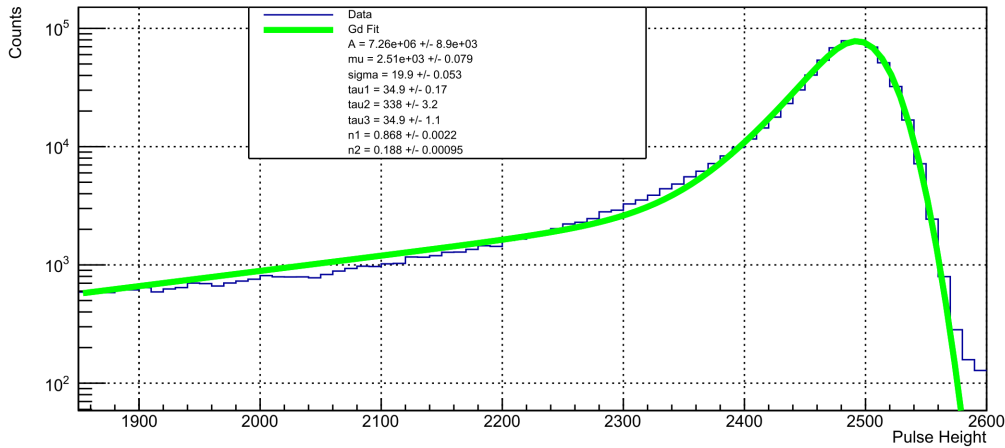

Figure 3.2: Logarithmic plot of the data shown in figure 3.1.

For ^{148}Gd the logarithmic plot shows slight deviations for the data in the region of the low energy tail. Overall both fits show unproblematic results, for further use in the calibration.
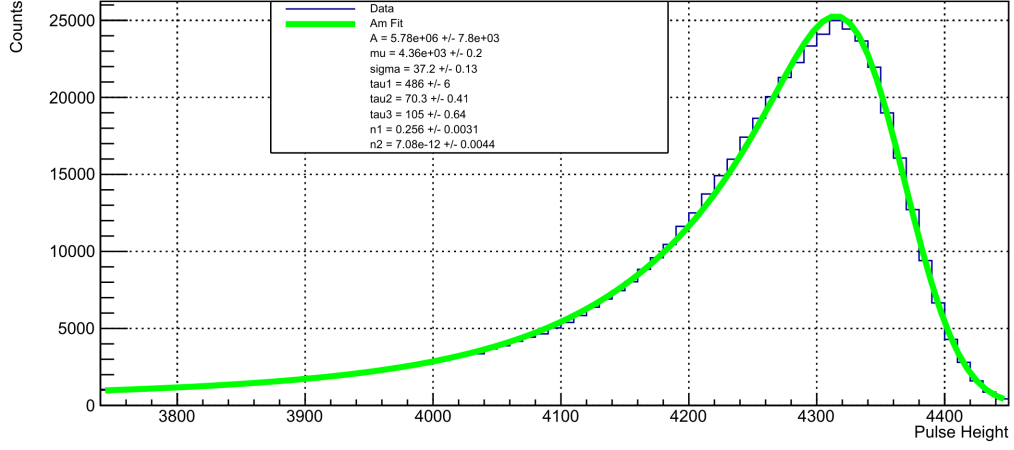
18

Figure 3.3: Histogram of the ^{241}Am peak, with the α-fit produced as described above.
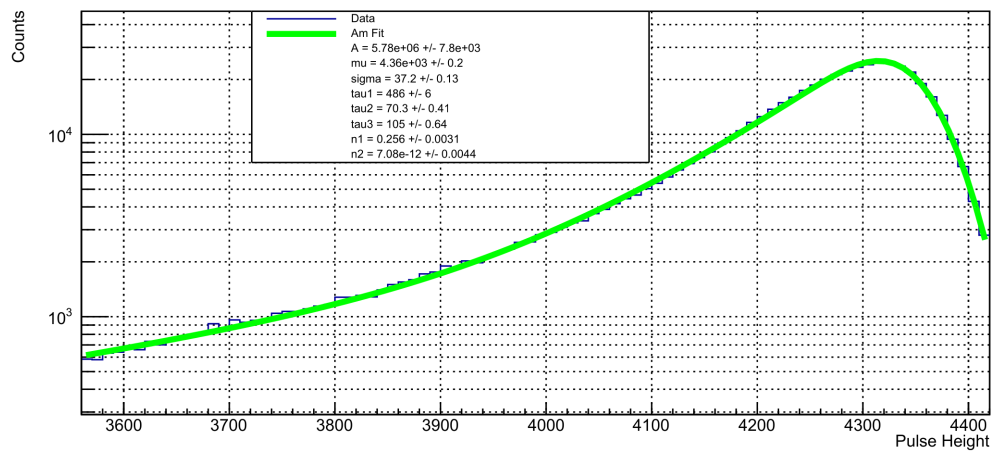

Figure 3.4: Logarithmic plot of the data shown in figure 3.1.

For the deviation several possible explanations. First it can be useful to consider the sample or the sample holder as a potential source of additional background. The samples are often used over long time periods and are exposed to the laboratory environment. This can lead to flaws in the structure and contamination on the surface, where the radioactive atoms are positioned. Even if the handling of the sample holders is assumed to be done with due care, the lab environment contains dusty areas and is therefore a factor, worth considering to improve. The most likely cause can be seen in chapter 5, where the background spectrum will be discussed. It will show a peak at the emission energy of ^{148}Gd covering 30 % of all background events after the data cuts are applied.

3.3   Obtaining the Calibration

The displayed pulse height directly corresponds to the energy of an α-particle, that was lost in the detector's gas volume due to ionization. The fit returns a value for the peak position. This parameter is used as the corresponding value to the particle energy, which is well known. The calibration is obtained applying a linear fit with an offset between the two data points of ^{148}Gd and ^{241}Am. Here the y-values are the energies and the x-values are the measured pulse heights. For the error of the x-values, the error of the peak position returned by the α-fit is used. The y-values (α-energies) are also found in literature [13]. A comprehensive evaluation of the resulting error, using an initial requiring an initial estimation before the calibration spectrum is fitted, is omitted. Since using only two sources for the measurement does not allow for the identification of potential non-linear behavior in the calibration data, this type of analysis would not contribute to a better understanding of the apparatus.

Isotope	$\mu/(10^3\text{ch})$	error/ch
^{148}Gd	2.51	0.081
^{241}Am	4.36	0.2

Table 3.1: Input pulse heights and errors for the calibration fit.

Isotope	E/ MeV	error/MeV
^{148}Gd	3,27121	0,00003
^{241}Am	5,63782	0,00012

Table 3.2: Input for the calibration fit: Literature values for α-energies and their error were given by [13].

The used fit function was

$$f(x) = a_1 x + a_0$$

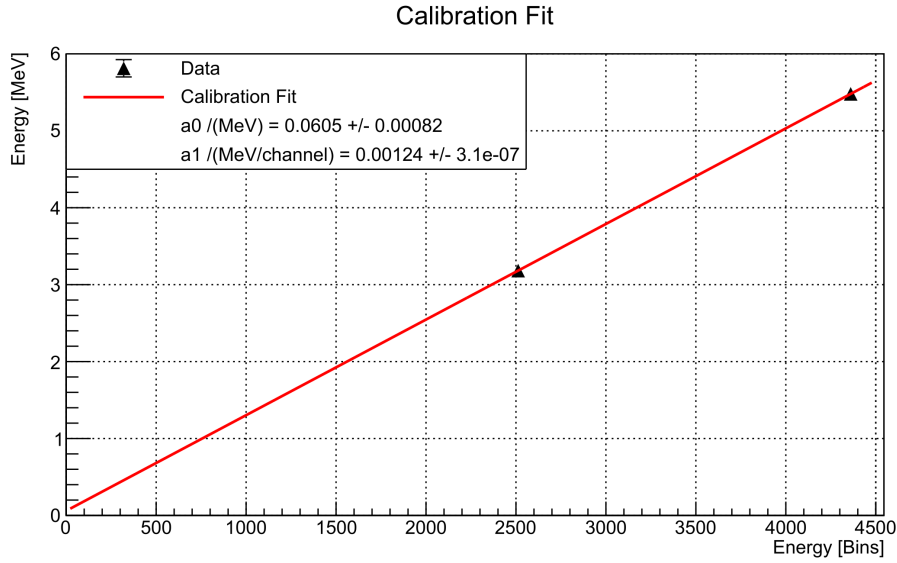The result can be seen in figure 3.5.

Figure 3.5: Calibration fit with the 2 data points ^{148}Gd and ^{241}Am.

3.4   Correcting for Measurement Time

In the measurements conducted over several days, the measured pulse heigths were found to decrease over time. Since the the energy of the α-particles remains the same, this is a clear sign for a technical problem in the setup. Several reasons for this problem were discussed and tested for. A lack could lead to gas exchange and therefore altering ionization energies. Another reason could be, that the chamber is not isolated so that charge would be trapped on the silicon wafer at the base. After runs with different modifications in the setup, for example removing the wafer completely, did not show an improvement, the existing calibration was adjusted. With the help of Christoph Seibt the calibration parameter a_1 was adjusted for every data package, containing the events of one hour, according to the drift in the pulse height.

4 Development of Correction Function for the Velocity Filter

In the condition to determine the validity of the data points by the average drift velocity of the corresponding electrons a correction is needed. As mentioned in section 2.2.5 the estimation for the velocity

$$v_e = \frac{D(1 - \frac{\bar{X}}{D}\cos\theta)}{T_A - T_{LG}} \tag{47}$$

uses the z-projection of the mean position of the cloud. To use the trigger times right, we have to consider the top of the cloud (in z-direction). To correct for this issue a energy dependent corrective function $a(E)$ is multiplied with the initial z-position, resulting in the product term estimating the top of the cloud at $t = 0$.

$$v_e = \frac{D(1 - a(E)\frac{\bar{X}}{D}\cos\theta)}{T_A - T_{LG}} \tag{48}$$

This section is describing the process of how this corrective function $a(E)$ was obtained. The series of steps was:

1. Simulation oft the ionization paths for altering energies.

2. Calculating the respective values for the center of charge. The top of the cloud is given by the simulation program.

3. Fitting the quotients $\frac{X_{max}}{X}$ resulting in $a(E)$

4.1 SRIM and TRIM Simulations

The simulation of the ionizations along the path of α-particles is done with the two softwares SRIM (Stopping and Range of Ions in Matter) and TRIM (the Transport of Ions in Matter) from 2013 was used [14][15]. Given the input parameters of ion type, gas composition and gas density, SRIM simulates the ranges of the specified ions for various energies. TRIM, on the other hand, requires ion energy as an additional input and simulates the energy loss due to ionization along the ions path using fine binning.

The α particles were simulated in TRIM at energies of $0.5\,\mathrm{MeV}$, $1\,\mathrm{MeV}$ and then in steps of $1\,\mathrm{MeV}$ up to $10\,\mathrm{MeV}$. SRIM computes the ion ranges for a range of energies, including these 11 specific values. The TRIM software also allows to choose the number of ions to be simulated per run. In this work, $10\,000$ particles were simulated for each selected energy.
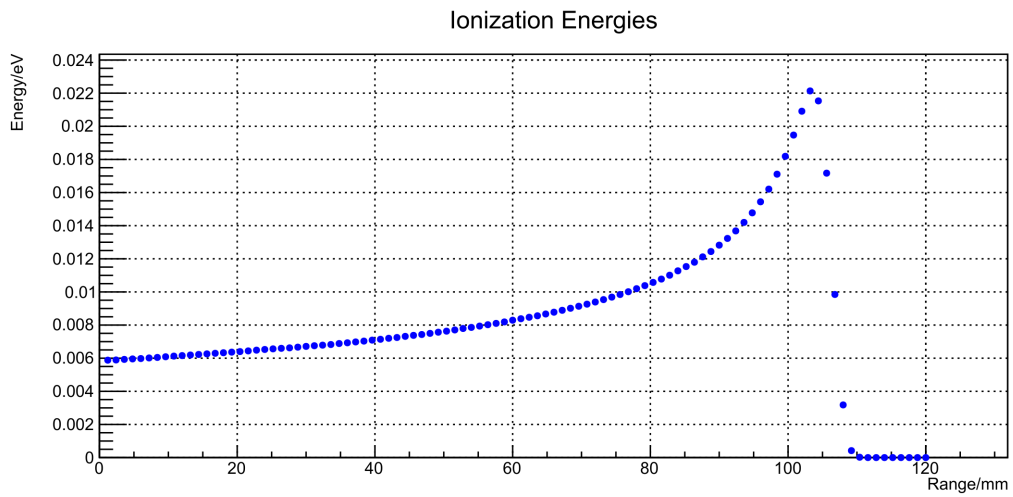
A visualization of the energy loss is shown in figure 4.1, illustrating the energy loss per bin and per particle for three example energies.
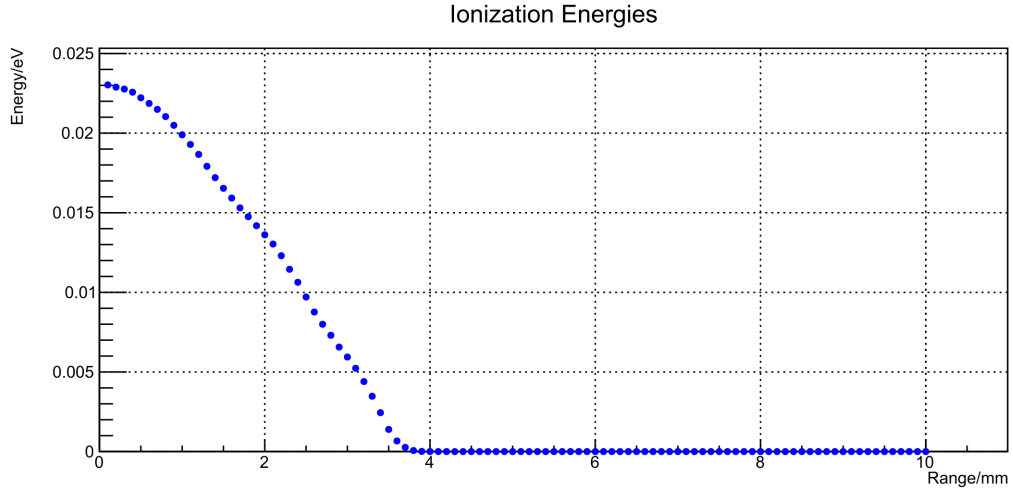
(a) Ionization, 0.5 MeV
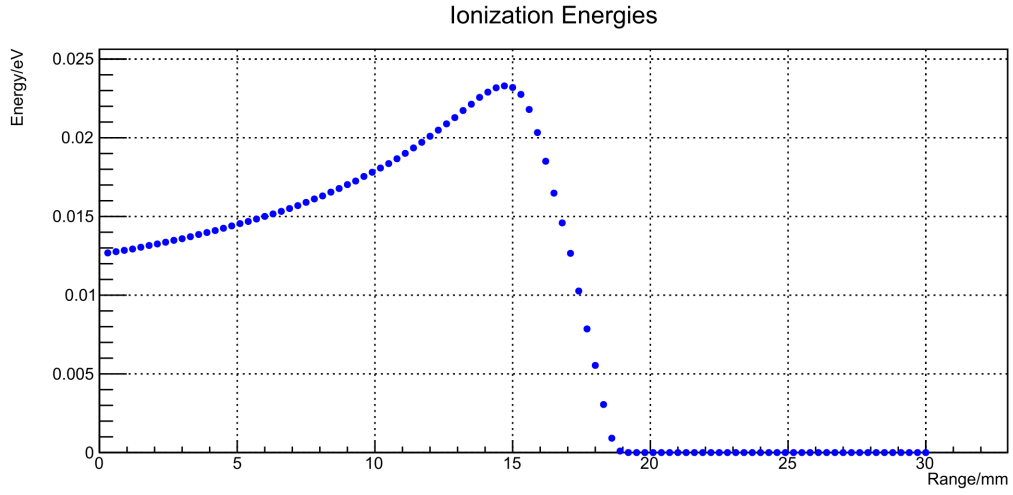
(b) Ionization, 3.0 MeV

(c) Ionization, 10.0 MeV

Figure 4.1: In this figure the the average energy deposition of 10000 α-particles over the path length is shown for 3 example energies. These results were obtained using the TRIM simulation software.

23

From the SRIM output the same energies and the corresponding ranges were selected. In this context, range means: range projected in z-direction. To get an understanding on how the range depends on the initial energy of the α-particle, the selected examples were fitted and plotted. This plot is shown in figure 4.2 .
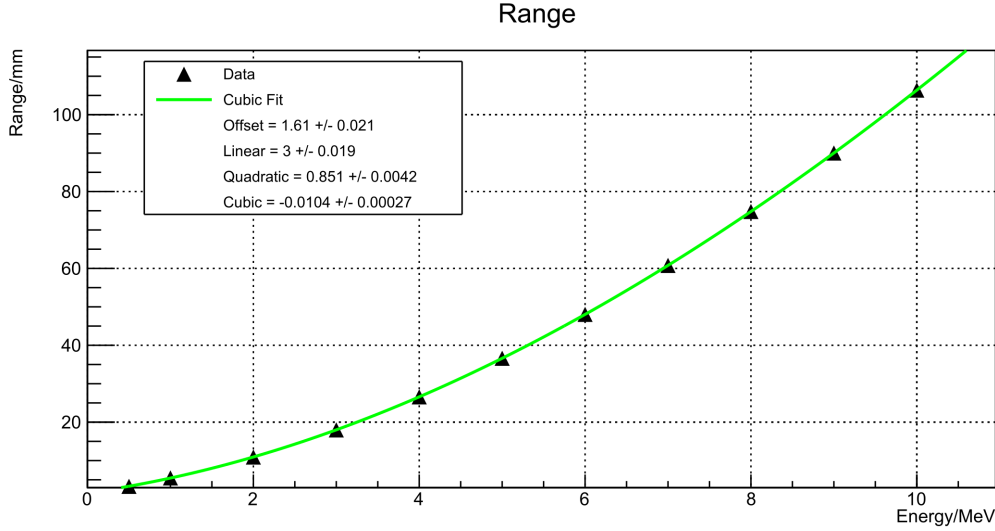

Figure 4.2: This image shows the ranges of α-particles in respect to the emission energy, simulated with SRIM. In addition the parameters for a cubic fit of the range can be seen.

4.2   The Center of Charge

The mean value for z, for every energy was calculated using:

$$\bar{X} = \frac{\sum_i x_i y_i}{\sum_i y_i} \tag{49}$$

After testing for different polynomial functions, again the 3rd degree fit was the first to show a good curve. The data for the center of charge can be seen in figure 4.3. The behavior of both curves seems to be similar. The most significant difference is that the peak position is increasing faster for higher energies.

4.3   Fitting the Quotiens

To finally obtain a corrective function, the quotients of range and center of charge were calculated for each energy that was simulated for. The result is depicted in fig 3.4. After testing for different types of functions, an exponential decrease with an offset proved to be most suitable. This is the same approximation as used in [8]. A visualization of the the quotients with the applied fit can be seen in fig 4.4.
The corrective factor converging to a constant value supports the decision to fit the two positions with polynomials $P(x)$ of the same degree, as their quotient also
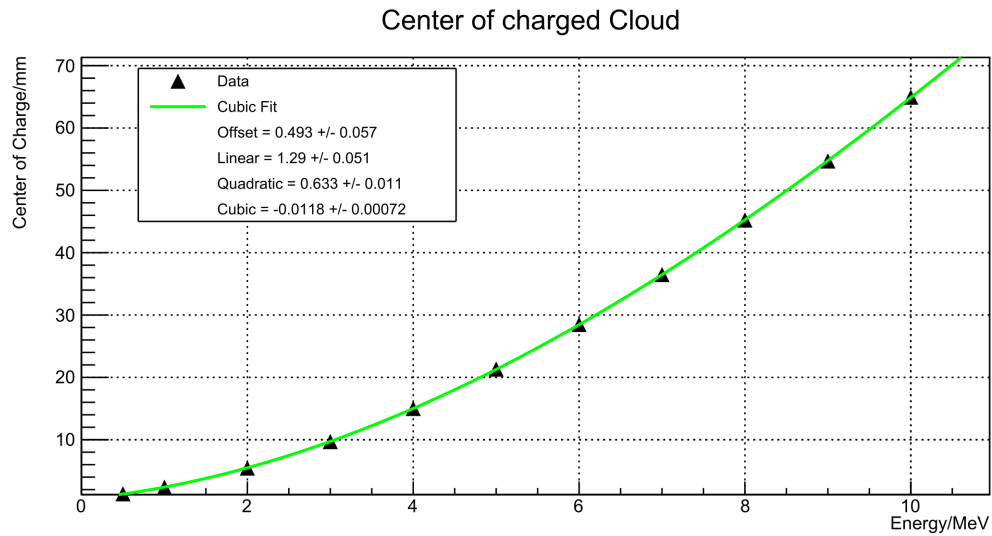
Center of charged Cloud

Figure 4.3: This image shows the calculated center of charge for every simulation run with the TRIM program. Like in the diagram before, a cubic fit was applied and shown.
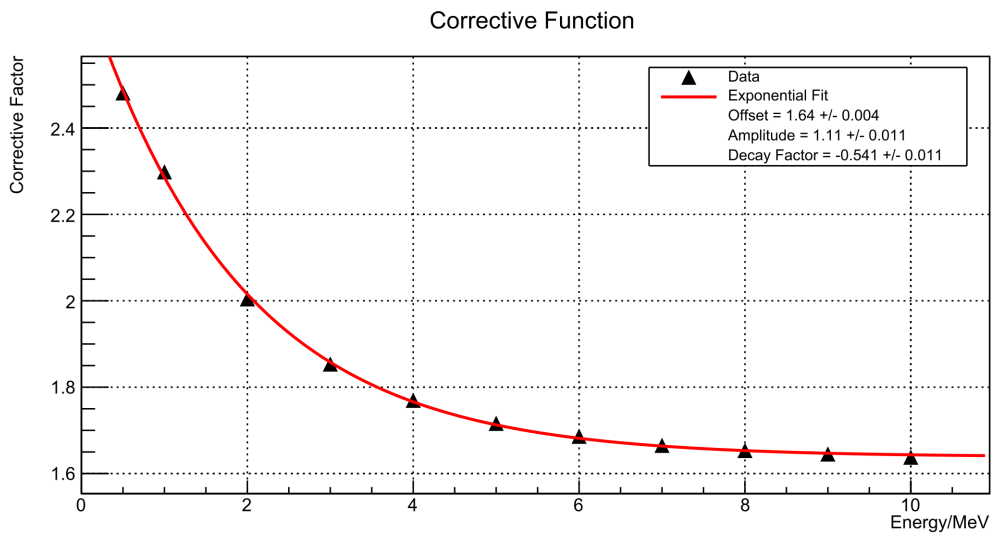
Corrective Function

Figure 4.4: The data points in this diagram are the ratios of the data points of the top of the cloud and the center of charge at the corresponding energies. The data is fitted as exponentially decaying with a positive offset.

approaches a constant value for $x \to \infty$. To make this comparison it is necessary that the quotients are taken from the raw data and the results are fitted afterwards. In conclusion, it can be stated that the chosen method provides a good approximation across all data points within the later investigated energy interval.

5   Background Analysis

One of the most important steps to prepare the α-chamber for a material screening is to conduct a measurement without a sample. This measurement of the background is needed for a correct interpretation of a measurement with a sample, because it allows to discriminate events stemming from the sample from the environmental background of the chamber. Also it is the first step in the search for contamination in the apparatus and its improvement.

The background measurement was conducted over a time period of 1000 h. Only with quality cuts the background showed 1000 counts per day. With quality cuts and physical cuts the rate was reduced to 85 counts per day.
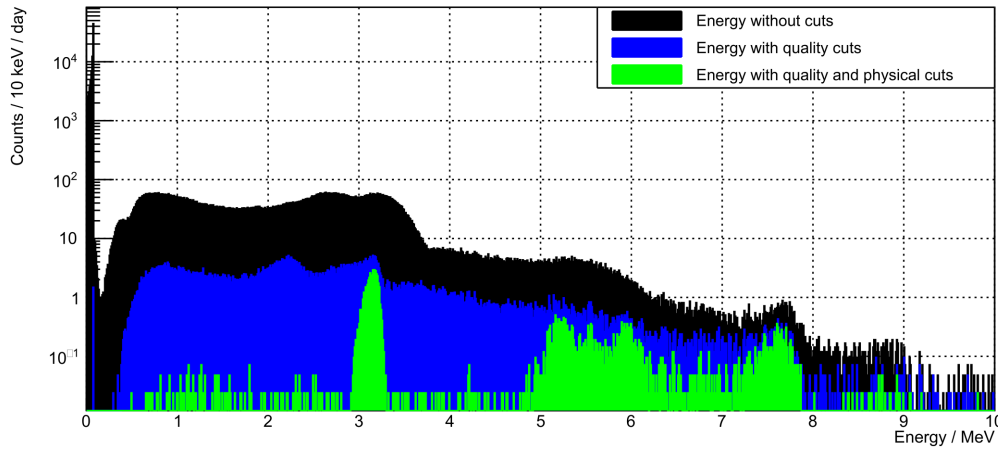

Figure 5.1: This image shows the entire background spectrum. It distinguishes between all events detected (black), the events that only passed the quality cuts (blue) and the events after every applied cut (green)

In figure 5.2 the entire background spectrum can be seen. It provides insight into the effectiveness of the implemented cuts. The quality cuts alone filter nearly 100 % of the events below 0.5 MeV. Above this energy two structures emerge. First a background noise between 0 and 10^{-1} counts per day in each 10 keV bin can be seen. It reaches from energies of 0.5 MeV up to 9 MeV. From 3 MeV upwards peak structures show. The data contains peaks at energies, that were seen in previous measurements 9 years ago [4], as well as a new structure at 3 MeV.

The peaks at 5 MeV and above can be associated with α-emitters, known to appear as contamination in the chamber. The data allows to distinguish between a single peak at $7 - 8$ MeV and three overlapping structures at $5 - 6$ MeV. At around 3 MeV a new contaminant, responsible for about $\frac{1}{2}$ of the background after cuts, can be seen. Table 5.1 shows all fitted positions of the identified peaks.

The separation of the three single peaks between 5 MeV and 6 MeV was only possible after introducing the time corrected calibration. It is to mention, that the data in
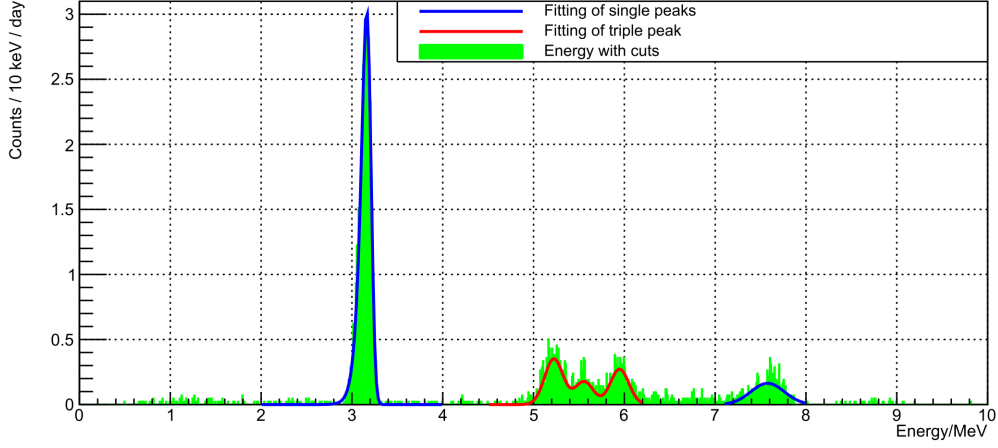
Figure 5.2: Here all background events after all cuts are shown. Also the fit functions of every identified peak can be seen.

Peak	μ/MeV	error/MeV
first single	3.208	0.006
triple 1	5.223	0.007
triple 2	5.557	0.010
triple 3	5.947	0.007
second single	7.577	0.013

Table 5.1: This table contains every fitted peak position and the corresponding error, resulting from the fit.

this area was not fitted using the aforementioned method and function designed for α-peaks. A lack of data probably causes the fit not to iterate properly based on the amount of degrees of freedom. Instead a triple gauss fit was used as a simplification. For the first component, the fitted peak position was $\mu_{t1} = 5.22\,\text{MeV}$. The energy indicates, that it represents α-particles emitted by ^{210}Po. This isotope is known in literature with an α-energy of $5.30\,\text{MeV}$. The second component peaked at $\mu_{t2} = 5.56\,\text{MeV}$ and is therefore most likely caused by ^{222}Rn emitting at $E_\alpha = 5.59\,\text{MeV}$. The third and last component with a peak at $\mu_{t3} = 5.95\,\text{MeV}$ can be associated with ^{218}Po, which is the daughter nuclide of ^{222}Rn.

A significant phenomenon here is, that the results all show deviations in the same direction and order of magnitude with respect to the literature value of the associated α-emitter. This can be explained by the usage of gaussian functions for the fit, as a gaussian distribution has the peak position at the maximum. In contrast, the peak value (energy) in an α-fit can be found slightly in positive x-direction compared to the maximum of the distribution. This explanation also applies to the following single peak at $\mu_{s2} = 7.58\,\text{MeV}$, which is matched to ^{214}Po with an α-energy of $E_\alpha = 7.69\,\text{MeV}$. The discussed nuclides are all part of the decay chain

of ^{222}Rn which itself is part of the decay chain of ^{238}U. ^{238}U and therefore ^{222}Rn are naturally occurring isotopes. Radon as a noble gas can be found in the atmosphere and is therefore expected to be found as a contamination, as well as the daughters of ^{222}Rn. The gaussian fits of the peaks, belonging to the ^{222}Rn chain can be seen in figure 5.3. The image clearly shows, how the gaussian peaks are aligned with the highest bins. On the one hand this shows, that the fit algorithm worked as it is supposed to and that the reduction to three fit parameters per peak improves the applicability. On the other hand it means that the energy is returned as the respective x-value of the maximum position, which creates a systematic error.
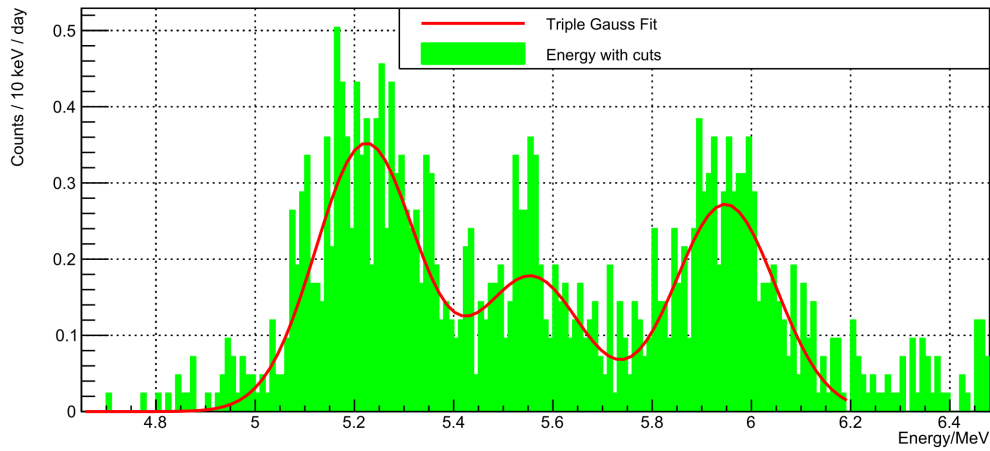

Figure 5.3: Background events after cuts. Energy range of the triple peak structure.
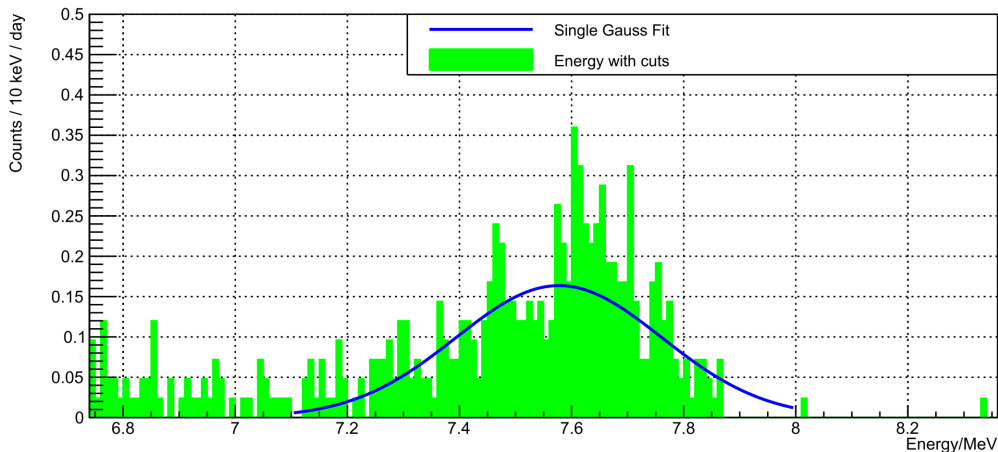

Figure 5.4: Background events after cuts. Energy around $7 - 8$MeV

The one peak left to discuss stands out for two reasons:

1. It contains by far the most counts, representing about $\frac{1}{2}$ of the whole background after cuts

2. It did not appear in any previous measurements, nor does its energy match any isotope in the expected decay chains.

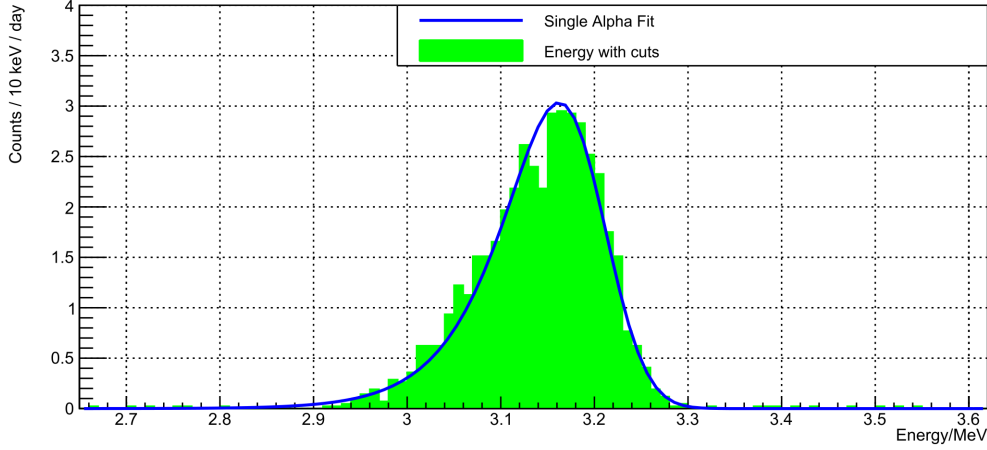The structure with the applied α-fit is shown in figure 5.5.

Figure 5.5: Background events after cuts. ^{148}Gd peak.

When a peak of this significance appears without any prior observation an artificial contamination must be suspected. For the calibration, samples with a very high α-activity were put inside the chamber. Because of the low range of α-particles in solid matter, the radioactive nuclei are brought onto the surface of the samples. Therefore, traces containing radioactive nuclei can easily be dragged off and cause contamination inside the chamber, especially the base next to the probe. An additional problem is that a central position at the bottom of the chamber is exactly, what the physical cuts do not veto. As mentioned in section 2.2.5, some events caused by contamination at the chamber wall will also pass the data filters. Therefore the the isotopes used for the calibration are checked first. The emission energy of ^{241}Gd $E_\alpha = 3.271\,\text{MeV}$ matches the peak position $\mu_{s1} = 3.208\,\text{MeV}$. In this the explanation of the usage of a compromised fit function does not apply, because an α-fit was applied.

At last the contents of the separate peaks, which can be seen in table 5.2, will be discussed.

Peak	content /counts per day
^{222}Rn	5.26
^{218}Po	8.11
^{214}Po	9.00
^{210}Po	10.48
^{148}Gd	43.75

Table 5.2: Count rates of all identified peaks.

6   Discussion and Outlook

6.1   Calibration

In general the calibration has put out useful results. The peaks in the measurement corresponded well to the structure of an α-peak. The fit only showed slight deviations in the tail region. Most importantly the calibrated spectrum matched the expected particle energies. It is to mention, that this evaluation applies after the time correction.

This is also the first point for future projects. The cause for the pulseheight drift over time is still to be found. As the tests for leaks and trapping of electric charge showed no convincing result, the most likely cause is outgassing from the walls. The effect of the release of gas trapped in the chamber walls should be further investigated by conducting a long term pressure measurement with an evacuated chamber. Another measure to improve the energy calibration should be to expend the underlying measurements to more than two calibration sources. This step is considered to be profitable for the entire experiment for three reasons. First the reliability and the precision of the result would increase. Second the knowledge of the structure of the calibration curve can only be obtained using multiple sources. Lastly the use of a polynomial function to fit two data points does not allow to return an useful uncertainty to the result, as the function will always perfectly match the data.

6.2   Corrective Function for the Velocity Filter

The structure of corrective function was chosen as it matches the data in the investigated energy scale well, using only three parameters. It has to be said, that if an experiment over greater energy scales was to be executed, the function might not represent the development of the corrective factor between the top of the charged cloud and its mean position anymore. However for the purposes pursued with this setup, the energy scale, the simulations were performed in, is not expected to be exceeded. The reason for this is, that while α-particles can have energies up to $12\,\mathrm{MeV}$, the emitters of these high energy alphas are very short lived. As the half live of these isotopes decreases drastically for higher Q-values, they are not relevant for long term experiments. Therefore work on a broadening of the applicability is considered not to have a high priority.

As the result is used to filter data based on the deviation from the expected values, a detailed analysis of the error of the simulations could be a good topic to work on.

6.3   Analysis of the Background Spectrum

The data gathered in the background spectrum allowed to identify the expected elements from the ^{238}U-chain (the daughters of ^{222}Rn) as well as a big structure caused by ^{148}Gd. Before the time correction it was not possible to identify any structures between 5 and 6 MeV. The modification of the calibration allowed to see a triple peak and identify the isotopes ^{222}Rn, ^{218}Po and ^{210}Po.

Still several structures above 6 MeV could not be identified. It is likely that these peaks are caused by ^{220}Rn and its daughter isotopes, which are part of the ^{232}Th decay chain. The biggest limiting factor here is considered to be the amount of data. To get a more detailed knowledge of the composition of the background spectrum a longer measurement would be useful. Also the energy drift, which could not be perfectly corrected caused smearing. Therefore the identification and elimination of its cause is considered as a rather high priority task.

Further the count rates of the identified sources suggest steps of cleaning. The first step, setting up a clean room tent is already in progress. This new environment is likely to prevent a big fraction of dust and other outside contaminants to enter the chamber in the process of a sample change. Another issue to be considered are the contaminants, which are already in the chamber. As the current data cuts allow events from the base and the walls of the chamber, these should be cleaned. A very simple measure would be to conduct a measurement, while the silicon wafer at the base of the chamber is turned around.

On a larger timescale the very effective steps would be to improve or create new cuts to guarantee filtering out events, not originating from the source and to test different methods for the determination of the pulseheight.

References

[1]   N. Abgrall, A. Abramov, N. Abrosimov, et al. "The large enriched germanium experiment for neutrinoless double beta decay (LEGEND)". In: *AIP Conference Proceedings.* Author(s), 2017. DOI: 10.1063/1.5007652.

[2]   M. Agostini, G. R. Araujo, A. M. Bakalyarov, et al. "Final Results of GERDA on the Search for Neutrinoless Double-β Decay". In: *Physical Review Letters* 125.25 (2020), p. 252502. DOI: 10.1103/physrevlett.125.252502.

[3]   Bethge. *Kernphysik, Eine Einführung.* Springer Berlin Heidelberg, 2008. DOI: 10.1007/978-3-540-74567-9.

[4]   A. Hartmann, J. Hutsch, F. Krüger, et al. "Design and performance of an ionisation chamber for the measurement of low alpha-activities". In: *Nuclear Instruments and Methods in Physics Research Section A: Accelerators, Spectrometers, Detectors and Associated Equipment* 814 (2016), pp. 12–18. DOI: 10.1016/j.nima.2016.01.033.

[5]   T. Mayer-Kuckuk. *Kernphysik.* Vieweg+Teubner Verlag, 2002. DOI: 10.1007/978-3-322-84876-5.

[6]   S. Tavernier. *Experimental Techniques in Nuclear and Particle Physics.* Springer Berlin Heidelberg, 2009. DOI: 10.1007/978-3-642-00829-0.

[7]   F. Sauli. *Gaseous Radiation Detectors: Fundamentals and Applications.* Cambridge University Press, 2022. DOI: 10.1017/9781009291200.

[8]   H. Wilsenach. "Long Live Alpha Decay". Doctoral dissertation. TU Dresden, 2021.

[9]   W. Shockley. "Currents to Conductors Induced by a Moving Point Charge". In: *Journal of Applied Physics* 9.10 (1938), pp. 635–636. DOI: 10.1063/1.1710367.

[10] S. Ramo. "Currents Induced by Electron Motion". In: *Proceedings of the IRE* 27.9 (1939), pp. 584–585. DOI: 10.1109/jrproc.1939.228757.

[11] Z. He. "Review of the Shockley–Ramo theorem and its application in semiconductor gamma-ray detectors". In: *Nuclear Instruments and Methods in Physics Research Section A: Accelerators, Spectrometers, Detectors and Associated Equipment* 463.1–2 (2001), pp. 250–267. DOI: 10.1016/s0168-9002(01)00223-6.

[12] S. Pommé and B. Caro Marroyo. "Improved peak shape fitting in alpha spectra". In: *Applied Radiation and Isotopes* 96 (2015), pp. 148–153. DOI: 10.1016/j.apradiso.2014.11.023.

[13]   IAEA. "Nuclear Data". In: (2014).

[14]   J. F. Ziegler and J. P. Biersack. *SRIM-2008, Stopping Power and Range of Ions in Matter.* 2008.

[15]   J. F. Ziegler, M. Ziegler, and J. Biersack. "SRIM – The stopping and range of ions in matter (2010)". In: *Nuclear Instruments and Methods in Physics Research Section B: Beam Interactions with Materials and Atoms* 268.11 (2010). 19th International Conference on Ion Beam Analysis, pp. 1818–1823. DOI: https://doi.org/10.1016/j.nimb.2010.02.091. URL: https://www.sciencedirect.com/science/article/pii/S0168583X10001862.

REFERENCES

Danksagung

First of all, I want to thank my referees Dr. Thomas Kormoll and Prof. Dr. Arno Straessner for reviewing my work and the help along the way. I am grateful for the opportunity to write my Bachelor´s theses at IKTP. I enjoyed the insight, I could get into low background experiments like the LEGEND experiment, as well as into the process of data analysis and the investigation on various kinds of problem sources and how to deal with them. Most enjoyable was getting to know the broad spectrum of solutions, reaching from newest technology to rather simple seeming tricks.

My sincerest gratitude goes to the entire nuclear physics group, which was a great environment to be in and offered help at every step of the way. Most importantly I need to thank Christoph Seibt. As my supervisor he gave insight into every important process, answered a lot of questions and supported me, whenever needed. I would also like to give a special thanks to Steffen Turkat, who provided kind help and useful opinions on many occasions.

Erklärung

Hiermit erkläre ich, dass ich diese Arbeit im Rahmen der Betreuung am Institut für Kern- und Teilchenphysik der Technischen Universität Dresden ohne unzulässige Hilfe Dritter verfasst und alle Quellen als solche gekennzeichnet habe.

Maximilian Cott
Dresden, 04.08.2025